International Journal of Digital Twin Systems and Computing (IJDTSC) ISSN: 3108–0790
DOI: https://doi.org/10.XXXXX/IJDTSC.2026.V2I204

Experimental Performance Assessment of a Micro Wind Energy Generator and a Charge-Controller-Based Framework for Residential DC Energy Management

[1]Pastin Jebamalai J, [2]Chithra S, [3]Stanly Selvakumar J, [4]Shajini Sheebha M E, [5]Jasmine J
[1]Student, [2,3,4,5]Assistant Professor
[1,2,3,4,5]Department of Electrical and Electronics Engineering, Stella Mary's College of Engineering, Aruthenganvillai, Kanyakumari District, Tamil Nadu 629202, India
[2]Corresponding Author Email: chithrasivathanulingam@gmail.com

Abstract: *This paper reports a bench-level performance assessment of a micro wind energy generator and develops a charge-controller-based framework for residential DC energy management built on the measured quantities. In the test configuration, a three-phase wind generator feeds a diode-bridge rectifier and a charge controller that supplies a DC load and a battery; measurements were taken at the charge-controller output. The recorded dataset–battery terminal voltage and current during a 'load running with battery only' test–is reported transparently together with the recomputed battery power, whose maximum is about 0.376 W. An important and openly stated limitation is that the dataset is sparse (five points, four sharing the same 0.04 A current) and that the DC-load and turbine three-phase quantities, as well as wind speed, were not logged; consequently the charge-controller efficiency that the experiment defines cannot be evaluated from the available data, and no efficiency value is fabricated. A pronounced drop of battery voltage from 22.4 V at open circuit to roughly 8.4–9.4 V under a 0.04 A load is identified and discussed as a likely high-source-impedance or near-depleted-source effect rather than concealed. The paper formalizes the wind-power, rectifier, power-balance, and efficiency relations; proposes an energy-management architecture coupling maximum power point tracking (MPPT), battery storage, and prioritized loads; and specifies exactly which additional measurements (load and turbine voltage and current, wind speed, and time stamps) are required to make the assessment fully quantitative. The contribution is a disciplined, end-to-end, fully traceable path from a limited teaching measurement to a deployable micro-wind energy-management concept.*

Keywords: Micro Wind Turbine, Permanent-Magnet Generator, Three-Phase Rectifier, Charge Controller, Maximum Power Point Tracking, Battery Storage, DC Microgrid, Energy Management.

Nomenclature

P_{wind}, P_m	Wind power available and mechanical power extracted (W).
ρ, A, v	Air density (kg/m^3), swept area (m^2), wind speed (m/s).
C_p, λ, β	Power coefficient, tip-speed ratio, pitch angle.
ω, R	Rotor angular speed (rad/s) and radius (m).
V_{dc}, V_{LL}	Rectified DC voltage and line-to-line voltage.
P_{turb}	Turbine/generator electrical power (W).
P_{bat}, P_{load}	Battery and DC-load power (W).
V_{bat}, I_{bat}	Battery terminal voltage (V) and current (A).
η_{cc}	Charge-controller efficiency (%).
D	Converter duty cycle.
SoC	Battery state of charge.

I. Introduction

Wind is among the fastest-growing renewable resources, and small or 'micro' wind turbines are attractive for distributed and residential generation because they can be installed close to the load and combined with battery storage to form a stand-alone DC supply [1, 4]. A micro wind energy conversion system (WECS) typically uses a permanent-magnet synchronous generator (PMSG) whose variable-frequency three-phase output is rectified to DC, conditioned by a charge controller, and used to charge a battery and run loads [5, 7].

The power available in the wind is strongly nonlinear–it varies with the cube of wind speed–so the operating point must be managed to extract useful power and to protect the battery during charging [2, 3]. A charge controller performs this conditioning, regulating charge and discharge and limiting current and voltage at the load. The performance of such a system is assessed by measuring the electrical quantities at each stage and computing the power delivered to the battery and the load.

This paper treats a standard micro-wind performance-assessment experiment as a measurement campaign and asks how its results feed a smart residential energy-management system (EMS). In doing so it is deliberately explicit about what the recorded data can and cannot support, which is the paper's defining discipline.

A. Research Gap

Teaching-laboratory micro-wind experiments often define efficiency formulas but record only a subset of the quantities those formulas require, while system-level WECS studies assume idealized sources. There is little work that carries a single, transparently reported (and admittedly limited) measured dataset through to an energy-management design while clearly separating measured facts, assumptions, and quantities that simply cannot be computed from the data.

B. Contributions

1) A transparent report of the recorded battery-side measurements with power recomputed from first principles, and an explicit account of the dataset's sparsity and anomalies.

2) A precise statement of why the experiment's defined charge-controller efficiency cannot be evaluated from the recorded data, and exactly which measurements are missing.

3) A consolidated set of governing relations (wind power, rectification, power balance, efficiency) for the micro-WECS.

4) A charge-controller-based EMS framework integrating MPPT, battery storage, and prioritized loads, with an explicit measurement plan for a fully quantitative future study.

C. Novelty Statement

The novelty is methodological: an end-to-end, fully traceable treatment in which every reported number is either measured, computed from the measurements, or explicitly flagged as an assumption or as indeterminate. This integrity–especially the refusal to manufacture an efficiency value the data cannot support–distinguishes the work from both typical lab reports and idealized WECS studies. Section II reviews related work; Section III gives the system model; Section IV the setup and methodology; Section V the results and their honest interpretation; Section VI the proposed framework; Section VII the performance discussion; and Sections VIII–IX future scope and conclusions.

II. Literature Review

Architecture and efficiency trade-offs for small wind turbines were studied in depth by Mirecki et al. [1], who compared control strategies and ac–dc conversion structures and showed that the operating point must be controlled to optimize the energetic behavior, especially when the $C_p(\lambda)$ characteristic is not known a priori. Teodorescu and Blaabjerg [2] demonstrated flexible control of small turbines in both stand-alone and grid-connected modes, which is directly relevant to a battery-backed residential system.

Maximum power point tracking for WECS has been surveyed extensively. Abdullah et al. [3] and Kumar and Chatterjee [4] review conventional and advanced trackers and consistently report perturb-and-observe (P&O) as the transparent baseline, with intelligent methods improving tracking under fast wind changes at higher complexity; a recent meta-heuristic study [5] reports tracking efficiencies above 99 % in simulation. Sensorless strategies that avoid mechanical sensors [6,7] and active-rectifier control for micro-wind systems [8] further reduce cost and improve robustness.

On the conversion chain, the PMSG–diode-bridge–boost arrangement used here is the most common low-cost topology [6]. Wind-turbine power-curve modeling [9] and high-efficiency small-turbine designs [10] provide the performance context, while controllers for grid-interconnected small turbines [11] and classic references on wind-energy integration [12] frame the system-level picture. These works generally assume well-instrumented sources; the present contribution is to anchor such a framework to a transparently reported–if limited–measured dataset. Table 1 summarizes representative works and the gap addressed here.

III. Micro Wind System Modeling

The kinetic power available in a wind stream passing through the rotor swept area A is

$$P_{wind} = \tfrac{1}{2}\, \rho\, A\, v^3 \tag{1}$$

where ρ is air density and v the wind speed. Only a fraction of this can be captured; the theoretical maximum is the Betz limit

$$C_{p,max} = \frac{16}{27} \approx 0.593 \tag{2}$$

so the mechanical power extracted by a real rotor is

$$P_m = C_p(\lambda, \beta)\, P_{wind} = \tfrac{1}{2}\, C_p\, \rho\, A\, v^3 \tag{3}$$

with the power coefficient C_p a function of the tip-speed ratio

$$\lambda = \frac{\omega R}{v} \tag{4}$$

and pitch angle β. The PMSG output is rectified by a three-phase diode bridge (Fig. 1), whose average DC output for an ideal bridge is

$$V_{dc} = \frac{3\sqrt{2}}{\pi}\, V_{LL} \approx 1.35\, V_{LL} \tag{5}$$

Table 1: Representative Related Work and Relation to This Study

Ref.	Year	Focus / scope	Method and validation	Relation to this work
[1]	2007	Small-wind architecture vs. efficiency	Comparative analysis of structures	Motivates operating-point control
[2]	2004	Stand-alone / grid small-turbine control	Control design; experiments	Battery-backed residential basis
[3]	2012	MPPT algorithms for wind	RSER review	P&O adopted as baseline
[4]	2016	Conventional + advanced wind MPPT	RSER review	Upgrade path beyond P&O
[6]	2012	Sensorless rotor-position control	PMSG, experiments	Low-cost control reference
[8]	2015	Active rectifier for micro-wind	IEEE TSE; integrated control	Conversion-stage reference
[9]	2014	Wind-turbine power-curve modeling	RSER review	Power-curve context (illustrative)
[5]	2025	Metaheuristic MPPT for WECS	Sci. Rep.; simulation	Recent tracking benchmark

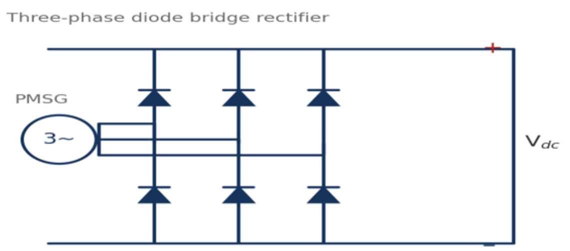

Figure 1: Three-phase diode-bridge rectifier converting PMSG output to DC.

The turbine/generator electrical power and the DC-side powers are

$$P_{turb} = V_{dc} I_{dc} \tag{6}$$

$$P_{bat} = V_{bat} I_{bat} \tag{7}$$

$$P_{load} = V_{load} I_{load} \tag{8}$$

Following the experiment, charge-controller efficiency is defined for the two operating cases as

$$\eta_{cc,\,turbine} = \frac{P_{bat} + P_{load}}{P_{turb}} \times 100\,\% \tag{9}$$

$$\eta_{cc,\,battery\text{-}only} = \frac{P_{load}}{P_{bat}} \times 100\,\% \tag{10}$$

These definitions require P_{load} and P_{turb}; Section V shows why they cannot be evaluated from the present dataset.

IV. Experimental Setup and Methodology

The system layout (Fig. 2) is a micro WECS in which a three-phase wind generator feeds a bridge rectifier and a charge controller; the controller output supplies a DC load and a battery, and an inverter with a filter supplies an AC load. As stated in the experiment, measurements are made at the charge-controller output, where DC power is available for battery charging and DC-load running. The apparatus is listed in Table 2, and the measurement points are shown in Fig. 3.

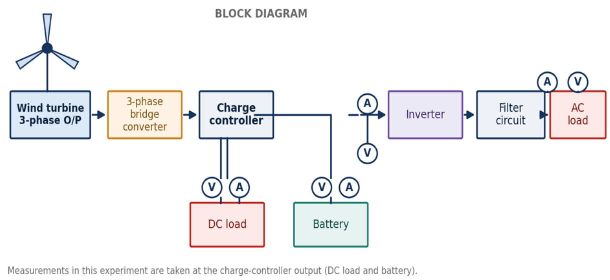

Figure 2: System block diagram of the micro wind energy generator with charge controller, battery, inverter, and loads.

Table 2: Apparatus Used in the Experiment

Apparatus	Type	Qty
Wind turbine set-up	—	1
3-phase bridge converter	—	1
Battery	—	1
Inverter	—	1
Voltmeter	—	1
Ammeter	—	1
Connecting wires	—	a/r

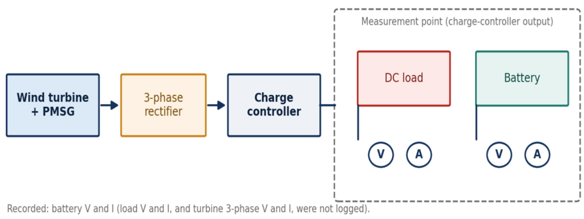

Figure 3: Measurement methodology: quantities are recorded at the charge-controller output.

A. Charge Controller Operation

The charge controller regulates battery charging and discharging and limits load current and voltage. A pulse-width-modulation (PWM) controller switches the charging current on and off at high frequency, providing a tapering charge: as the battery voltage rises toward full charge, the on-time of each pulse shortens, reducing the average current into the battery (Fig. 4). The experiment's manual states a conversion efficiency above 90 % for such controllers; this is the device's typical specification, not a quantity measured here.

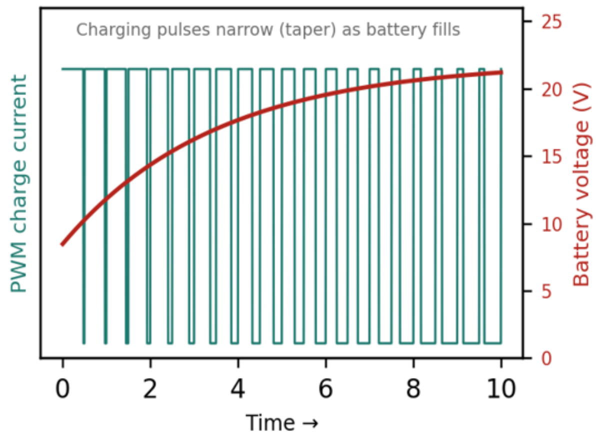

Figure 4: PWM charge-controller behavior: charging pulses taper as battery voltage rises.

B. Procedure

1) Assemble the chain: turbine → 3-phase rectifier → charge controller → DC load and battery; connect the inverter–filter–AC-load branch.

2) At the charge-controller output, record voltage and current of the battery (and, in a complete study, of the DC load).

3) Compute battery power as $P = V \cdot I$; the experiment may be run with battery only, or with battery and turbine together.

V. Results and Discussion

Table 3 lists the recorded observations for the 'load running with battery only' case, with battery power recomputed as $P = V \cdot I$. The arithmetic in the original log is consistent: the maximum recorded battery power is about 0.376 W. These are sub-watt levels, indicating a near-idle or very low wind condition during the bench test.

Table 3: Measured Battery Data (Load Running with Battery Only)

No.	I (A)	V (V)	P = V·I (W)
1	0.00	22.4	0.000
2	0.04	9.4	0.376
3	0.04	8.9	0.356
4	0.04	8.4	0.336
5	0.04	8.6	0.344

A. Observations and an Honest Reading of the Data

Two features of the dataset must be stated plainly. First, the data are sparse: only five points were recorded and four of them share the same 0.04 A current, so the battery-side behavior is captured at essentially a single operating current (Fig. 5). Second, the battery voltage falls sharply from 22.4 V at open circuit (zero current) to about 8.4–9.4 V once a small 0.04 A current flows (Figs. 5 and 6). A drop of this magnitude at such a low current implies a very high effective source impedance and is consistent with a nearly depleted or weakly excited source, or with the measurement being taken at a point that is not the battery terminals alone. It is reported as-is rather than smoothed, because it materially affects any power or efficiency interpretation.

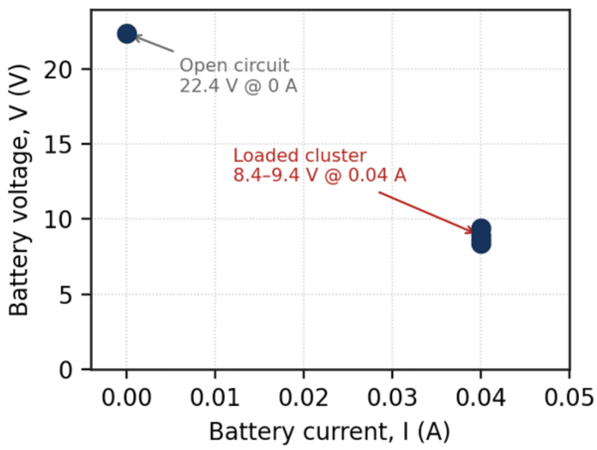

Figure 5: Battery voltage versus current: open-circuit point and the loaded cluster at 0.04 A.

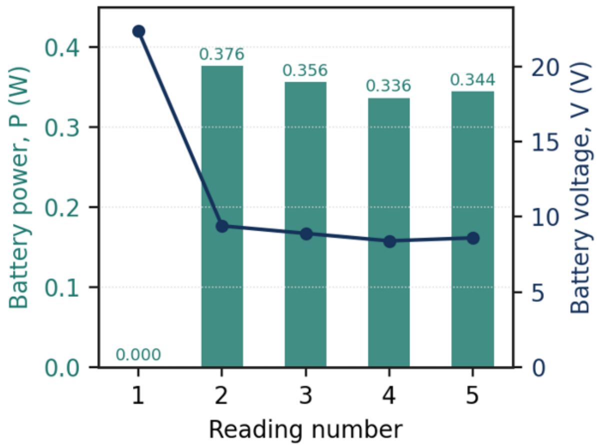

Figure 6: Battery voltage and recomputed power across the five recorded readings.

B. Why Charge-Controller Efficiency Cannot Be Computed Here

The experiment defines charge-controller efficiency through (9) and (10), which require the DC-load power P_{load} and the turbine power P_{turb}. The recorded observations contain only battery voltage and current; load voltage/current and the turbine three-phase voltage/current were not logged, and wind speed was not measured. Therefore neither efficiency expression can be evaluated, and no efficiency figure is reported. Table 4 separates, explicitly, what is measured, what is computed, and what is indeterminate with the present data. This is a limitation of the dataset, not of the method, and Section VIII lists the measurements needed to close it.

Table 4: What the Data Supports: Measured, Computed, and Indeterminate Quantities

Quantity	Value	Status
Battery OC voltage	22.4 V	measured
Battery loaded voltage	8.4–9.4 V	measured
Battery current	0 / 0.04 A	measured
Battery power (max)	0.376 W	computed
DC-load power	—	not recorded
Turbine power	—	not recorded
Wind speed / C_p	—	not measured
Charge-ctrl. efficiency	—	indeterminate

C. Power-Curve Context (Illustrative Only)

Because wind speed was not recorded, no measured power curve or power coefficient can be produced from this experiment. For context only, Figs. 7 and 8 show the standard theoretical shapes–a cube-law power curve with cut-in, rated, and cut-out regions, and a $C_p(\lambda)$ curve bounded by the Betz limit. These are illustrative references drawn from the model of Section III and the literature [9], not results of this experiment, and they are labeled as such in the figures.

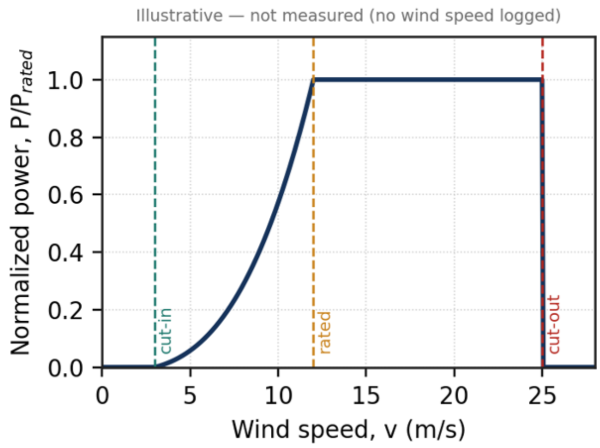

Figure 7: Illustrative wind-turbine power curve (not measured; no wind speed was logged).

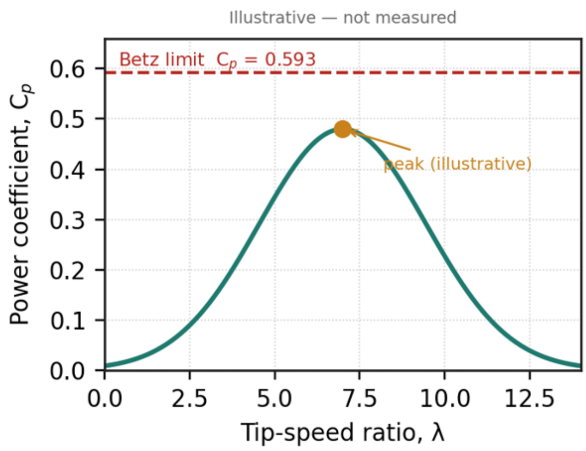

Figure 8: Illustrative $C_p(\lambda)$ curve bounded by the Betz limit (not measured).

VI. Proposed Energy-Management Framework

The measured chain motivates a charge-controller-based EMS (Fig. 9) in which an MPPT stage maximizes captured wind power, a battery buffers the mismatch between generation and demand, and loads are served by priority. The fast inner loop is MPPT; the slower outer loop is energy scheduling.

DOI: https://doi.org/10.XXXXX/IJDTSC.2026.V2I204
ISSN: 3108–0790

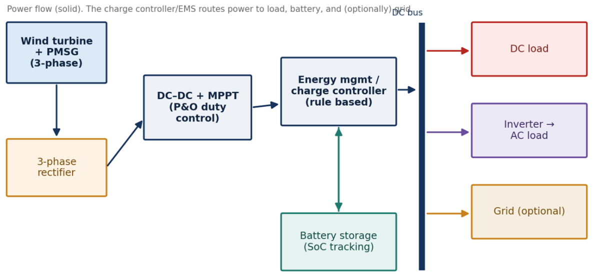

Figure 9: Proposed micro-wind energy-management architecture coupling PMSG, rectifier, MPPT converter, charge controller, battery, and prioritized loads.

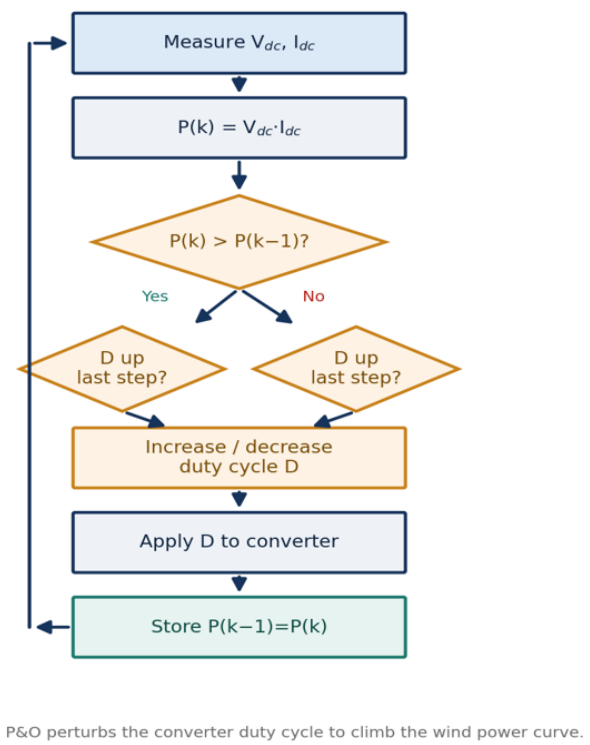

Figure 10: Perturb-and-observe MPPT control flow on the DC-side power.

A. Maximum Power Point Tracking

Because the wind power curve has a single maximum at each wind speed, a perturb-and-observe (P&O) controller perturbs the converter duty cycle and observes the change in DC power [3, 4]:

$$D(k+1) = \begin{cases} D(k) + \Delta D, & \dfrac{\Delta P}{\Delta D} > 0 \\ D(k) - \Delta D, & \dfrac{\Delta P}{\Delta D} < 0 \end{cases} \qquad (11)$$

If a perturbation increases power, the next keeps direction; otherwise it reverses. The P&O steps are summarized in Fig. 10; sensorless and intelligent trackers [5–7] can replace this block without changing the architecture.

B. Battery Storage and Power Balance

At the controller node the powers balance as $P_{turb} + P_{bat} = P_{load}$, where a positive battery term denotes discharge (Fig. 11). The battery state of charge evolves as

$$SoC(t + \Delta t) = SoC(t) - \frac{\eta_c P_{bat}(t)\, \Delta t}{E_{cap}} \qquad (12)$$

so the battery absorbs surplus wind power and supports the load when generation is insufficient, decoupling generation from demand in time [2, 8].

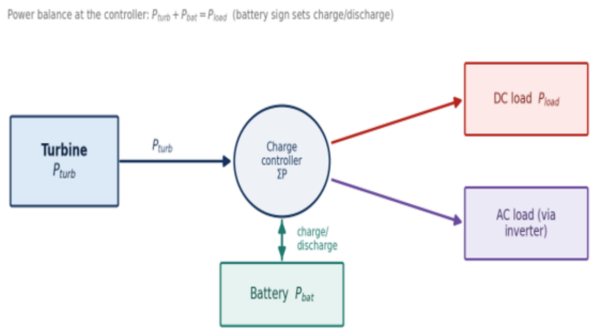

Figure 11: Power balance among turbine, battery, and loads at the charge controller.

C. Load Prioritization

Loads are tagged by priority: critical DC loads are served first; deferrable loads are scheduled into periods of surplus wind or high state of charge; non-essential loads are shed first under deficit. With the battery and MPPT in place, the controller aims to maximize the share of wind energy used locally and to keep critical loads supplied during lulls, which is the central objective of a residential micro-wind EMS [2, 11].

VII. Performance Evaluation

A fully quantitative evaluation requires time-series wind speed, load, and turbine/load electrical data that were not part of this experiment. What can be stated now is structural and is summarized in Table 5: the measured battery behavior fixes the DC-side operating range, the governing relations of Section III fix the conversion limits (including the Betz bound), and the literature establishes the direction and typical magnitude of the benefits that MPPT and storage provide [1, 4, 8]. Table 6 gives an illustrative benefit sketch whose numbers are explicitly assumptions drawn from the cited literature, not measurements or guarantees.

Table 5: Qualitative Benefits of the Proposed System

Feature	**Benefit**	**Basis**
MPPT (P&O)	Keeps operation near the wind power-curve peak as wind varies	[3, 4]
Battery storage	Buffers gusts/lulls; supplies loads during calm periods	[2, 8]
Load prioritization	Keeps critical DC loads supplied; defers flexible loads	[2]
Charge control	Protects battery; tapered PWM charging near full SoC	manual / [8]

Table 6: Illustrative Figures (Assumptions / Specs, Not Results)

Item	**Illustrative value**	**Status**
Betz upper bound	$C_p \leq 0.593$	theoretical limit
MPPT gain vs. fixed load	+10–30 %	assumed range [3, 4]
Tracking efficiency (sim.)	up to ∼99 %	reported in [5]
Charge-ctrl. efficiency	>90 %	device spec, not measured

Values are theoretical limits, literature ranges, or device specifications included to indicate direction and order of magnitude only. They are not measured in this experiment and must not be read as performance guarantees.

VIII. Future Scope

Record the missing electrical quantities. Log DC-load voltage/current and the turbine three-phase voltage/current so that P_{load} and P_{turb}, and hence the charge-controller efficiencies (9)–(10), become real results.

Instrument the wind input. Add an anemometer to record wind speed v so that a measured power curve and $C_p(\lambda)$ can replace the illustrative curves of Figs. 7–8.

Densify and time-stamp the sweep. Record many operating currents over time, not a single 0.04 A point, to characterize the battery and DC-side behavior properly.

Investigate the voltage collapse. Diagnose the 22.4 V → ∼8.8 V drop (source state, internal resistance, connection/measurement point) and re-measure at the true battery terminals.

Dynamic EMS validation. Drive the architecture of Fig. 9 with time-series wind and load data and quantify captured-energy gain, self-sufficiency, and battery cycling.

IX. Conclusion

A micro wind energy generator was assessed at the charge-controller output. From the recorded 'battery-only' data, the battery power was recomputed (maximum ≈0.376 W), and a pronounced open-circuit-to-loaded voltage drop (22.4 V to about 8.4–9.4 V at 0.04 A) was identified and discussed transparently. Crucially, because DC-load power, turbine power, and wind speed were not logged, the charge-controller efficiency defined by the experiment cannot be computed, and no efficiency value was fabricated; the measured, computed, and indeterminate quantities were separated explicitly. The governing wind-power, rectification, power-balance, and efficiency relations were consolidated, and a charge-controller-based EMS integrating P&O MPPT, battery storage, and prioritized loads was proposed, with illustrative power-curve context clearly labeled as non-measured. The paper's value lies in its disciplined, end-to-end traceability from a limited measurement to a deployable micro-wind energy-management concept, and in the concrete measurement plan needed to make the assessment fully quantitative.

Acknowledgment

The author thanks the laboratory staff for assistance with the experimental setup.

References

[1] A. Mirecki, X. Roboam, and F. Richardeau, "Architecture complexity and energy efficiency of small wind turbines," *IEEE Trans. Ind. Electron.*, vol. 54, no. 1, pp. 660–670, Feb. 2007.

[2] R. Teodorescu and F. Blaabjerg, "Flexible control of small wind turbines with grid failure detection operating in stand-alone and grid-connected mode," *IEEE Trans. Power Electron.*, vol. 19, no. 5, pp. 1323–1332, Sep. 2004.

[3] M. A. Abdullah, A. H. M. Yatim, C. W. Tan, and R. Saidur, "A review of maximum power point tracking algorithms for wind energy systems," *Renew. Sustain. Energy Rev.*, vol. 16, no. 5, pp. 3220–3227, 2012.

[4] D. Kumar and K. Chatterjee, "A review of conventional and advanced MPPT algorithms for wind energy systems," *Renew. Sustain. Energy Rev.*, vol. 55, pp. 957–970, 2016.

[5] K. M. AboRas, M. H. EL-Banna, A. I. Megahed, and M. R. Hammad, “Optimal maximum power point tracking strategy based on greater cane rat algorithm for wind energy conversion system,” *Sci. Rep.*, vol. 15, 2025. DOI: 10.1038/s41598-025-18710-7.

[6] W. Qiao, X. Yang, and X. Gong, “Wind speed and rotor position sensorless control for direct-drive PMG wind turbines,” *IEEE Trans. Ind. Appl.*, vol. 48, no. 1, pp. 3–11, Jan./Feb. 2012.

[7] J. Brahmi, L. Krichen, and A. Ouali, “A comparative study between three sensorless control strategies for PMSG in wind energy conversion system,” *Appl. Energy*, vol. 86, no. 9, pp. 1565–1573, Sep. 2009.

[8] G. Buticchi, E. Lorenzani, F. Immovilli, and C. Bianchini, “Active rectifier with integrated system control for microwind power systems,” *IEEE Trans. Sustain. Energy*, vol. 6, no. 1, pp. 60–69, Jan. 2015.

[9] M. Lydia, S. S. Kumar, A. I. Selvakumar, and G. E. Prem Kumar, “A comprehensive review on wind turbine power curve modeling techniques,” *Renew. Sustain. Energy Rev.*, vol. 30, pp. 452–460, 2014.

[10] T. Matsushima, S. Takagi, and S. Muroyama, “Characteristics of a highly efficient propeller type small wind turbine with a diffuser,” *Renew. Energy*, vol. 31, no. 9, pp. 1343–1354, 2006.

[11] T. García-Sánchez, A. K. Mishra, E. Hurtado-Pérez, R. Puché-Panadero, and A. Fernández-Guillámon, “A controller for optimum electrical power extraction from a small grid-interconnected wind turbine,” *Energies*, vol. 13, no. 21, 2020.

[12] S. Heier, *Grid Integration of Wind Energy Conversion Systems*, 2nd ed. Chichester, U.K.: Wiley, 2006.